Method for reconstructing the self-energy from the spectral function

B. Sriram Shastry *

Physics Department, University of California, Santa Cruz, California 95064, USA

(Received 21 August 2024; accepted 9 October 2024; published 22 October 2024)

A fundamental question about the nature of quantum materials such as high-T_c systems remains open to date: it is unclear whether they are (some variety of) Fermi liquids, or (some variety of) non Fermi liquids. A direct avenue to determine their nature is to study the (imaginary part of the) self-energy at low energies. Here we present a method to extract this low-ω self-energy from experimentally derived spectral functions. The method seems suited for implementation with high-quality angle-resolved photoemission data. It is based on a helpful theorem proposed here, which assures us that the method has minimal (or vanishing) error at the lowest energies. We provide numerical examples showing that a few popular model systems yield distinguishably different low-energy self-energies.

DOI: 10.1103/PhysRevB.110.155149

I. INTRODUCTION

In this work we address the basic problem of reconstructing the low-energy $\mathrm{Im}\,\Sigma(\vec{k}_F, \omega)$ from the spectral function $A(\vec{k}, \omega)$ inferred from angle resolved photoemission experiments (ARPES). We refer to this as the inversion problem in this work. The ARPES probe of quantum materials [1] is known to play a vital part in our understanding of the important class of strongly correlated materials. The low-ω dependence of this object for $\vec{k} \sim k_F$ is of especial interest in theoretical studies, since reliable high-precision measurements, if available, would provide an essential direction in the search for a suitable theory for systems with strong correlations, and possibly also for superconducting states. Physically the low-ω object is directly related to the decay rate of a slightly excited particle near the ground state, and also can be used to infer a significant contribution to the T dependence of the resistivity of the system at low T.

An overarching question posed by numerous experimental results on strongly correlated systems, is whether these can be described using standard methods of condensed matter physics, or if not, whether they demand substantial revisions of the otherwise highly successful standard theory. The latter is based on the density functional theory of Kohn *et al.* as a starting point, and by treating the effects of interactions using perturbative expansions in the spirit of Landau's Fermi-liquid theory. Its validity can be questioned if the interactions become very strong, leading to much debate in the community. To sharpen the debate one chooses the most sensitive class of experimental results, and sees whether the predictions of standard theory are violated, and if so to what extent. Much emphasis so far has been on the temperature-dependent resistivity, which indeed has surprising and unexpected aspects in many strongly correlated systems. However, the theoretical calculation of the resistivity has considerable intrinsic complexity, being a higher-order correlation function involving two electrons and two holes. Therefore the evaluation of the (formally exact) Kubo formula for resistivity can only be done approximately, the difficulty being exacerbated when the interaction scales are large. Additionally there are system-dependent details at play, such as the different T dependences at different densities. Altogether these factors seem to prevent rigorous conclusions from being drawn on the question we started with, in either direction. On the other hand, the relatively simpler single electron and one hole spectral function contains crucial information about the low-energy and low-temperature dependence of the lifetime of a particle excited above the ground state. Extracting or accessing the most relevant pieces of information from the ARPES data is, however, a nontrivial task. This goal has been achieved at a certain level of accuracy, using an elaborate collation of energy dependence of spectral data at fixed wave vectors as described below. The purpose of this work is to introduce a new and direct method for this task, using an exact but rarely used formula for the self-energy in terms of the spectral function Eq. (3), (4). We also show that this method becomes increasingly accurate—even asymptotically exact—at lowest energy. By applying this method to a quantum material studied in its normal state, we could unravel essential details of its low-energy behavior, and thus ascertain whether it is a Fermi liquid or a quantum liquid of some other sort, and thereby provide definitive answers to the initially posed question.

A. Current status of the inversion problem

At present a few works report such an inversion. Important recent examples are given in Refs. [2,3]. The original effort of Ref. [2] uses the direct relationship between the spectral function as a function of the self-energy:

$$A(\vec{k}, \omega) = \frac{-1}{\pi} \frac{\mathrm{Im}\,\Sigma(\vec{k}, \omega)}{[\omega + \mu - \varepsilon_k - \mathrm{Re}\Sigma(\vec{k}, \omega)]^2 + [\mathrm{Im}\,\Sigma(\vec{k}, \omega)]^2}, \tag{1}$$

*Contact author: sriram@physics.ucsc.edu

and therefore at a fixed ω the width of a peak Δk_w is given by

$$\hbar v_k^{\text{eff}} \Delta k_w \sim 2\text{Im}\,\Sigma(\vec{k},\omega), \tag{2}$$

where v_k^{eff} is a renormalized velocity, so that the left-hand side may be roughly estimated from experiments. This inversion problem of reconstructing $\text{Im}\,\Sigma(\vec{k},\omega)$, requires the collation of data from several constant energy sections of the spectra function, termed the momentum distribution curves (MDC). A second method is presented in Ref. [3], which uses a novel momentum-energy resolved tunneling method, and demonstrate its working for two-dimensional electron systems embedded in a semiconductor. This important class of materials appears to be ideally suited for that method.

B. A proposal for inversion

The present work discusses a different framework for effecting this inversion, and provides some examples of how it can be used. In the following instead of the imaginary part of the self-energy $\text{Im}\,\Sigma(\vec{k},\omega)$, we discuss the equivalent but more convenient positive definite spectral density of the self-energy, obtained from $\rho_\Sigma(\vec{k},\omega) = -\frac{1}{\pi}\text{Im}\,\Sigma(\vec{k},\omega)$. We begin with an exact but apparently infrequently used [4] relation

$$\rho_\Sigma(\vec{k},\omega) = \frac{A(\vec{k},\omega)}{\{\Phi_{\vec{k}}(\omega)\}^2 + \{\pi A(\vec{k},\omega)\}^2} \tag{3}$$

$$\Phi_{\vec{k}}(\omega) \equiv \fint d\nu \frac{A(\vec{k},\nu)}{\omega-\nu}, \tag{4}$$

where $A(\vec{k},\omega)$ is the ARPES-related spectral function, $\Phi_{\vec{k}}(\omega)$ is the real part of the Green's function Eq. (A15), and $\fint$ represents a principal value integration (see Appendix A for details). We see from Eqs. (3), (4) that $\rho_\Sigma(\vec{k},\omega)$ is a functional of $A(\vec{k},\nu)$. If the overall scale of $A(\vec{k},\omega)$ is unknown, as is usually the situation in experiments, we can only hope to obtain ρ_Σ up to an overall constant. The nonlocality (in frequency) of Eq. (4) presents the main obstacle in this route of inversion. Although $A(\vec{k},\omega)$ is experimentally available for a range of ω near a peak [5], it seems from Eqs. (3), (4) that we need more. The Hilbert transform term $\Phi_{\vec{k}}(\omega)$, requires a knowledge of $A(\vec{k},\nu)$ at *all* ν in order to determine ρ_Σ rigorously. Any error in the estimated $\rho_\Sigma(\vec{k},\omega)$ therefore arises only from errors in evaluating $\Phi_{\vec{k}}(\omega)$ due to a limited (partial) knowledge of $A(\vec{k},\omega)$.

On closer inspection, we find that the situation is sensitively dependent on the regions of $\vec{k},\omega$ probed. We summarize our observation about achieving highest accuracy in estimating ρ_Σ as:

Theorem 1 (on highest accuracy inversion). As the energy is lowered to zero, errors in the Hilbert transform term $\Phi_{\vec{k}}(\omega)$ are of diminishing consequence to $\rho_\Sigma(\vec{k},\omega)$.

To understand the origin of this theorem, consider the following. If we allow for an error $\delta\Phi_{\vec{k}}(\omega)$ at a fixed $\vec{k}$ in the estimation of $\Phi_{\vec{k}}(\omega)$, the resulting fractional error in $\rho_\Sigma(\vec{k},\omega)$ to the first order is given by

$$\frac{1}{\rho_\Sigma(\vec{k},\omega)}\left|\frac{\delta\rho_\Sigma(\vec{k},\omega)}{\delta\Phi_{\vec{k}}(\omega)}\right| = 2\sqrt{\frac{\rho_\Sigma(\vec{k},\omega)}{A(\vec{k},\omega)}}\sqrt{1-\pi^2 A(\vec{k},\omega)\rho_\Sigma(\vec{k},\omega)} \tag{5}$$

$$\leqslant 2\sqrt{\frac{\rho_\Sigma(\vec{k},\omega)}{A(\vec{k},\omega)}}. \tag{6}$$

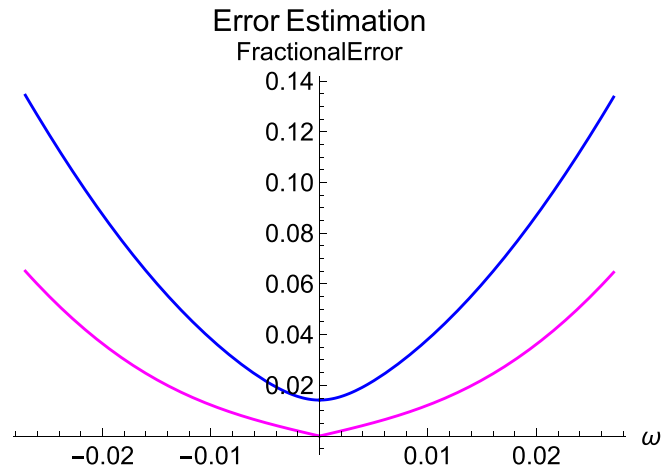

FIG. 1. The fractional error Eq. (5) (bottom magenta curve) and its upper bound Eq. (6) (top blue curve) for the asymmetric Fermi-liquid model Eq. (11) with parameters specified below in Eq. (15). Here ω is in units of eV as per the model. We note that the bound would also vanish at $\omega = 0$ if we use a vanishing elastic scattering energy η in Eq. (15).

In Fig. 1 we illustrate the fractional error and its upper bound given in Eqs. (5), (6) for the asymmetric Fermi-liquid model Eq. (11) defined below. For $\vec{k} \sim \vec{k}_F$ and $\omega \sim 0$, the spectral function $A(\vec{k},\omega)$ has a peak, and the self-energy term $\rho_\Sigma(\vec{k},\omega)$ is expected to vanish at $T = 0$ in disorder-free Fermi systems. The expression Eq. (5) can also be written as $2|\text{Re}\,G(\vec{k},\omega)|\frac{\rho_\Sigma(\vec{k},\omega)}{A(\vec{k},\omega)}$, which provides further understanding of the vanishing at $\omega = 0$, in terms of the expected vanishing of $\text{Re}\,G(\vec{k}_F,\omega\sim 0)$. The cumulative effect is that the fractional error and its upper bound Eq. (6) are least in the low-energy regime. This regime is also the most interesting one from a physical standpoint, since it defines the asymptotic low-energy physics of the system, where the behavior of the self-energy is an important characterization of the physics of the system. Therefore the above theorem provides a strong motivation to explore the approximate evaluation of Eq. (3), as a way to probe fundamental aspects of interacting Fermi systems.

Encouraged by the above discussion, we propose that this method for extracting the electron self-energy deserves some experimental effort. We can state our proposal in qualitative terms as follows: at a fixed $\vec{k}$ (chosen say as $\vec{k}_F$), the low-energy behavior of $\rho_\Sigma(\vec{k}_F,\omega)$, can be found from a knowledge of $A(\vec{k}_F,\omega)$ in a range of energies sufficiently close to its

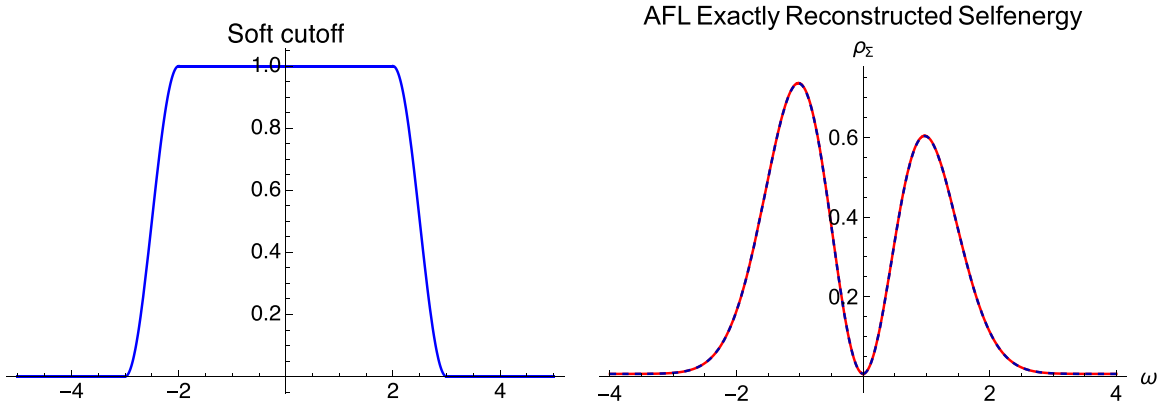

FIG. 2. These figures are for the asymmetric Fermi-liquid model Eq. (11) with parameters given in Eq. (15). Left: The soft cutoff function $\mathcal{T}(\omega)$ in Eq. (9) is illustrated with parameters $\{2, 3\}$ and $\Omega_* = 1$. Right: The initial $\rho_\Sigma(\vec{k}_F, \omega) + \frac{\eta}{\pi}$ from Eqs. (37), (38) (dotted blue) is exactly reproduced numerically (red), using the full energy window Hilbert transform to evaluate $\int d\nu \frac{A(\vec{k},\nu)}{\omega-\nu}$ in Eq. (3). It also agrees with the analytical calculation in Eq. (A12), showing the consistency of the starting point Eq. (3). A similar calculation performed away from $\vec{k}_F$ (as mentioned in the beginning of Sec. II) works equally well.

peak from Eq. (3) supplemented with a suitable frequency windowing of $A(\vec{k}_F, \omega)$. By frequency windowing we mean replacing $A(\vec{k}_F, \omega)$ in Eq. (3) as

$$A(\vec{k}_F, \omega) \to A'(\vec{k}_F, \omega) \equiv \mathcal{T}(\omega) A(\vec{k}_F, \omega), \tag{7}$$

and $\mathcal{T}(\omega)$ is a smooth symmetric function of ω, falling from 1 to zero smoothly beyond a suitable cutoff energy Ω_*. Examples of useful forms of $\mathcal{T}(\omega)$ are provided below. This procedure can also be carried out for arbitrary $\vec{k}$ away from $\vec{k}_F$ with $A'(\vec{k}, \omega) = \mathcal{T}(\omega - \omega_{\vec{k}}) A(\vec{k}, \omega)$ where ω_k is the location of the peak in $A(\vec{k}, \omega)$.

Clearly the proposal is not completely rigorous. The possibility of higher-order terms in $\delta\Phi_{\vec{k}}$ becoming dominant must be kept in mind while drawing conclusions from the above linear analysis based theorem. We provide numerical examples below that address this aspect of the problem. The examples displayed below suggest that in certain cases, the procedure leads to a reasonable reconstruction in the low-energy regime where it is increasingly accurate- in accordance with the theorem. In a variety of physically interesting examples, we start with a self-energy and construct the spectral function from it. We then use the spectral functions cutoff at some energy scale, following the lines suggested in the proposal, from which we reconstruct the self-energy. Comparing the reconstructed and original self-energies gives us useful insights. In the examples that are provided, it seems that the presence of a sharp peak in $A(\vec{k}, \omega)$ is helpful, as the Theorem 1 suggests. The utilization of the values of $A(\vec{k}, \omega)$ in a range of energies around the peak discussed below, yields an excellent picture of the low-energy behavior of the self-energy.

C. Cutoff functions

We suggested above the use of a windowed version of $A(\vec{k}, \omega)$ as in Eq. (7). In choosing to cutoff the frequency at a specific Ω_*, typically $\Omega_* \sim \nu W_0$, i.e., a few times the width of the spectral peak W_0, we must specify the cutoff function $\mathcal{T}(\omega)$. In taking the Hilbert transform, it seems useful to consider alternate forms of the cutoff.

We tested a sharp cutoff function

$$\mathcal{T}_{\text{Hard}}(\omega) = \Theta(\Omega_* - |\omega|), \tag{8}$$

where Ω_* is the cutoff energy. We also used a cutoff function, inspired by the Tukey window in Fourier transforms, that seems more promising. This piecewise function determined by the cutoff scale Ω_* and two positive numbers $\nu_- < \nu_+$, in terms of which we define

$$\begin{aligned}\mathcal{T}(\omega)|_{\{\nu_- W_0, \nu_+ W_0\}} &= 1 \quad \text{for } |\omega| < \nu_- W_0 \\ &= \frac{1}{2}\left(1 + \sin\frac{\pi}{2}\left\{\frac{1 + \nu_+ - 2|\omega|/W_0}{\nu_+ - 1}\right\}\right) \\ &\quad \text{for } \nu_- W_0 < |\omega| < \nu_+ W_0 \\ &= 0 \text{ for } \nu_+ W_0 \leqslant |\omega|. \end{aligned} \tag{9}$$

This function is displayed in Fig. 2. The scale W_0 is taken in most figures as the width (FWHM) of the spectral function, typical values of the ν numbers are $\nu_- \sim 3$ and $\nu_+ \sim 6$. Results for both windows are compared below in Fig. 4. While they agree at the lowest energies, in accord with the theorem, the comparison suggests that the window in Eq. (9) is somewhat better as we go away from $\omega = 0$. Without making any claim to its being optimal, we only use the window in Eq. (9) for further results.

II. EXAMPLES OF SELF-ENERGY INVERSION IN THREE MODEL SYSTEMS

In order to explore this problem of partial range reconstruction, we study three self-energy models next. We also set $\vec{k} = \vec{k}_F$ in this part of the work, this is the simplest case where Δk in Eq. (A9) and Eq. (A11) can be set at zero. Calculations for $\vec{k} \neq \vec{k}_F$ can be done in exactly the same way, by shifting the peak in the cutoff function Eq. (9) from 0 to $\delta\vec{k}$, the location of the spectral function peak. We comment on this in Fig. 2. Each model is given in terms of an explicit positive definite

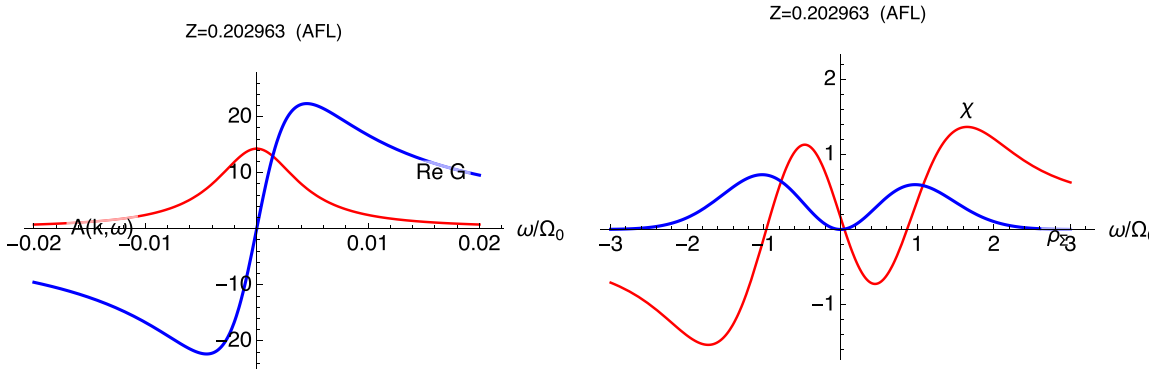

FIG. 3. These figures are for the asymmetric Fermi-liquid model Eq. (11) with parameters given in Eq. (15). Left: The spectral function $A(\vec{k}_F, \omega)$ and the Re $G(\vec{k}_F, \omega)$. Right: The imaginary self energy $\rho_\Sigma(\vec{k}_f, \omega)$ and $\chi(\vec{k}_F, \omega)$ for the A-FL model Eq. (11), calculated from Eqs. (41), (38), (48), using parameters given in Eq. (15). Here the spectral peak width W_0 is ∼9 meV.

self-energy $\rho_\Sigma(\vec{k}_F, \omega)$ dependent on a few parameters, and having a finite integral over ω.

The three illustrative models considered are expressed [see Eq. (B1)] in terms of dimensionless (scaled) frequency $\bar{\omega} \equiv \frac{\omega}{\Omega_0}$, a dimensionless temperature $\bar{\tau} = \frac{\pi k_B T}{\Omega_0}$, a dimensionless interaction strength parameter $\bar{\epsilon}_0 = \frac{\epsilon_0}{\Omega_0}$. In the case of the first model we also use $\bar{A} = \frac{A}{\Omega_0}$, it is a dimensionless asymmetry parameter. We also use the dimensionless version of ρ_Σ

$$\bar{\rho}_\Sigma(\vec{k}_F, \bar{\omega}) = \frac{1}{\Omega_0}\rho_\Sigma(\vec{k}_F, \omega), \tag{10}$$

where Ω_0 is the large energy scale. The relationship between Ω_0 and the spectral peak width W_0 is determined by uninteresting details of the model used. For example, changing the confining well from the Gaussian to another form in Eqs. (11)–(14) would change that relation. Therefore we choose $\Omega_0 = 1$eV and adjust other parameters so that the experimentally observable width (FWHM) W_0 of the peak at $\omega \sim 0$ is about 10 meV. These peak widths seem to be typical values for the scales for many high-T_c materials [1,2]. The three models, chosen for their proximity to interesting physical cases as well as for analytical tractability in a few cases, are defined by three choices of $\bar{\rho}_\Sigma$

$$\text{(asymmetric FL) } \bar{\rho}_\Sigma(\vec{k}_F, \bar{\omega}) = \epsilon_0(\bar{\tau}^2 + \bar{\omega}^2)(1 - \alpha\bar{\omega})e^{-\bar{\omega}^2} \tag{11}$$

$$\text{(marginal-FL-a) } \bar{\rho}_\Sigma(\vec{k}_F, \bar{\omega}) = \epsilon_0 \text{Max}[\bar{\tau}, |\bar{\omega}|]\, e^{-\bar{\omega}^2} \tag{12}$$

$$\text{(marginal-FL-b) } \bar{\rho}_\Sigma(\vec{k}_F, \bar{\omega}) = \epsilon_0(\bar{\tau} + |\bar{\omega}|)\, e^{-\bar{\omega}^2} \tag{13}$$

$$\text{(non-FL) } \bar{\rho}_\Sigma(\vec{k}_F, \bar{\omega}) = \epsilon_0\left(\bar{\tau}^{\frac{3}{2}} + |\bar{\omega}|^{\frac{3}{2}}\right)e^{-\bar{\omega}^2}. \tag{14}$$

These models are a nonexhaustive subset of the models discussed in literature, and chosen to provide a fairly broad diversity of behavior. The low-frequency behavior of these models are of special interest, where the Gaussian term $e^{-\bar{\omega}^2}$ is essentially unity. This term is a confining well, chosen to provide a fall off at high $\bar{\omega}$ needed for the integrability of the spectral density. Other choices of the confining well are possible but unlikely to make a difference at low-$\bar{\omega} \ll 1$, which is the region of our main concern.

In Eq. (11) the chosen asymmetric FL function (A-FL in the following) describes an asymmetric Fermi liquid, where the first term $(\bar{\tau}^2 + \bar{\omega}^2)$ represents a Fermi liquid (FL), while the second term $(1 - \alpha\bar{\omega})$ generates a cubic asymmetric term

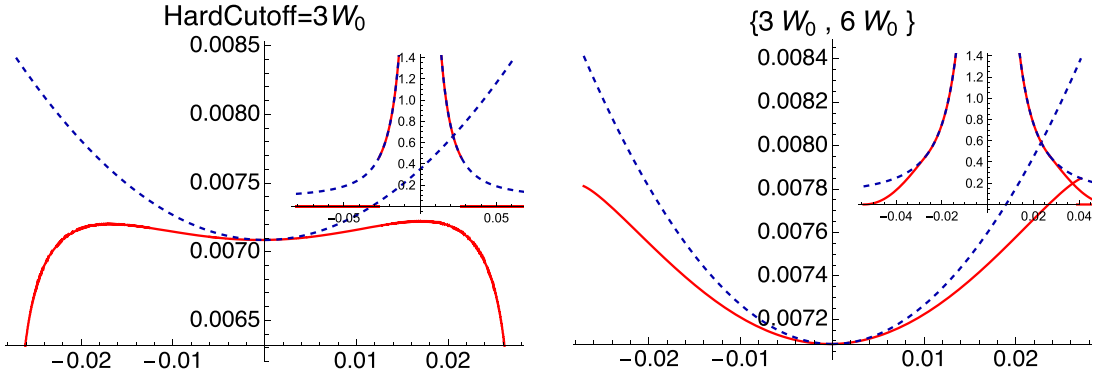

FIG. 4. These figures are for the asymmetric Fermi-liquid model Eq. (11) with parameters given in Eq. (15). The reconstructed self-energy $\rho_\Sigma(\vec{k}_F, \omega) + \frac{\eta}{\pi}$ (red curve) using on left a hard cutoff Eq. (8) and on right using the soft cutoff Eq. (9) compared with the exact value in the dashed blue curves. The two parameters relating to the soft cutoff Eq. (9) on right are indicated in curly brackets. The two insets show the exact spectral function in dashed blue and the cutoff included spectral function A' of Eq. (7) in the red curves. Here W_0 is ∼9 meV. On the left, while the hard cutoff does give a shallow minimum near $\omega \sim 0$, it is seen to turn around and become convex rapidly. The soft cutoff remains concave up to $3W_0$, and has a maximum (fractional) error of ∼6% at the maximum displayed energy $\omega = 3W_0$.

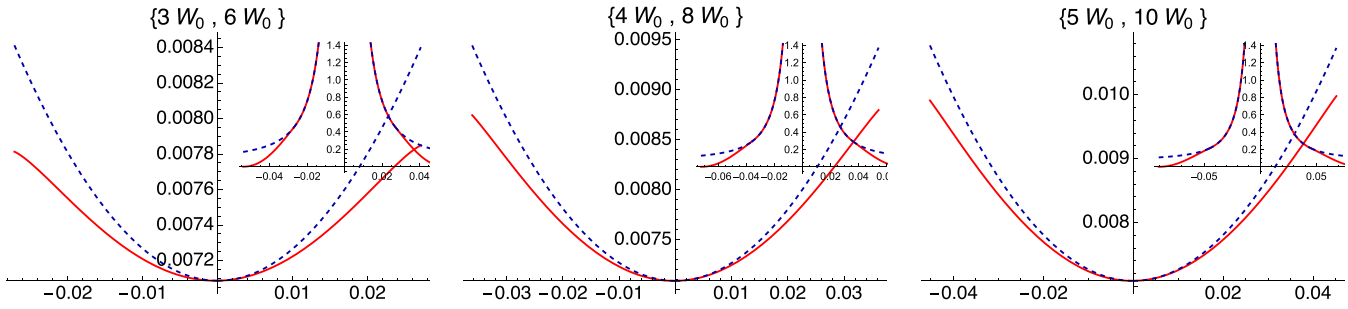

FIG. 5. These figures are for the asymmetric Fermi-liquid model Eq. (11) with parameters given in Eq. (15). The reconstructed self-energy $\rho_\Sigma(\vec{k}_F, \omega) + \frac{\eta}{\pi}$ (red curves) using the soft cutoff Eq. (9) compared with the exact value in the dashed blue curves. The two parameters relating to the soft cutoff Eq. (9) are indicated in curly brackets. The three insets show the exact spectral function in dashed blue and the cutoff included spectral function A' of Eq. (7) in the red curves. Here upper cutoff is twice the lower one. Increasing the magnitude of the cutoff is seen to reduce the error. Here W_0 is ∼9 meV.

in the self-energy. This model is a crude representation of the solution of the t-J model in two dimensions using the extremely correlated Fermi-liquid theory (ECFL) [7] at the lowest temperatures, if the parameters are chosen appropriately. The resistivity of this model is quadratic in T at the lowest temperature, and crosses over to a T-linear behavior at a very low crossover temperature [7]. This subtle crossover behavior requires the addition of terms of higher order in ω, and is buried in the T dependence of the coefficients. These details are not necessary for the basic analysis here, in this work we will provide a framework from which only the lowest-order quadratic behavior, on display in Eq. (11), might be tested in future experiments. The spectral function can be calculated fully in terms of the Dawson function D_F Eq. (B11), these and other necessary details are collected in Appendix B.

In Eqs. (12), (13) we consider two variants of the popular marginal Fermi liquid (M-FL in the following) model self-energy [8]. As in other models considered, the added exponential term is unity for $|\bar{\omega}| \ll 1$. The M-FL phenomenology builds in a T-linear resistivity in a natural fashion. The model M-FL-b Eq. (13) is in the same spirit as model M-FL-a Eq. (12), and leads to slightly different results at the lowest energy.

In Eq. (14) the chosen non-FL function (N-FL in the following) describes a non-Fermi-liquid system with a power law $|\omega|^{\frac{3}{2}}$, where the resistivity is expected to behave as $T^{\frac{3}{2}}$. While there appears to be no compelling argument for this specific choice of the power law $\frac{3}{2}$ used in our choice, we use it as an archetype of a strongly non-Fermi liquid of the type suggested in Ref. [9]. We adjust the parameters for these models so that the spectral function has about the same width W_0 of ∼10 meV in all cases.

In summary, in the following we follow these steps:

(1) For each model we use Eqs. (20), (29) to construct χ, and $A(\vec{k}, \omega)$.

(2) We then multiply A with a window function $\mathcal{T}(\omega)$ in Eq. (9), which vanishes smoothly beyond a frequency scale. This scale is chosen in most cases as Ω_*, a suitable multiple of W_0, the width (FWHM) of the spectral function. This process represents the selection of a small energy window and yields A' as in Eq. (7).

(3) From A' replacing A and Eqs. (31), (33), we construct $\rho_\Sigma(\vec{k}, \omega, \Omega_*)$, which now depends on our choice of Ω_*. We then compare with the parent value $\rho_\Sigma(\vec{k}_F, \omega)$, for $|\omega| \lesssim \Omega_*$.

As a check on the numerics and the formalism, we note that the two self-energies must agree when $\Omega_* \to \infty$. We present an example in Fig. 2 to demonstrate this agreement.

A. Asymmetric Fermi-liquid model

The parameters defined in Eq. (B1) are chosen for the following figures are

$$\epsilon_0 = 1.8,\ \alpha = 0.1;\ \eta = 0.02;\ \tau = 0.02;\ \alpha_z = 1.74, \quad (15)$$

where α_z Eq. (A4) corresponds to a filling $n = 0.85$, leading to a fairly low value of the quasiparticle weight $Z = 0.203$. The energies are given in units of Ω_0 chosen to be 1 eV for high-T_c systems. The value of η used here corresponds to typical laser ARPES experiments [10], while τ, the physical temperature $T = \tau/\pi \sim 74$ K. The width (FWHM) of the spectral function at these parameters is W_0 is ∼9 meV. We present figures showing the spectral function and self-energy for the A-FL model in Fig. 3. We further demonstrate the validity of the basic Eq. (3) for the A-FL model. In Fig. 2 we show the exact reconstruction of the self-energy from the spectral function using the Hilbert transform over all frequencies.

We present a comparison in Fig. 4 of the reconstruction schemes using two window functions: (i) A hard cutoff $\mathcal{T}(\omega) = \Theta(3W_0 - |\omega|)$ at an energy cutoff equaling thrice the FWHM of the spectral peak W_0 and (ii) the soft window given in Eq. (9) with parameters $\{3W_0, 6W_0\}$. In the caption we we comment further on the relative merits of the two schemes. In the two figures Figs. 5, 6 we display the reconstructed self-energy compared to the exact self-energy for different sets of the cutoff window parameters, and comment on their relative merits.

B. Marginal Fermi-liquid model

For the M-FL-a model, the parameters used are

$$\epsilon_0 = 1.8, \quad \eta = 0.02, \quad \tau = 0.01; \alpha_z = 1 \quad (16)$$

leading to a width $W_0 = 12$meV, which is only slightly bigger than $W_0 = 9$ meV for the A-FL model. The spectral function and the real part of the Green's function are shown in Fig. 7,

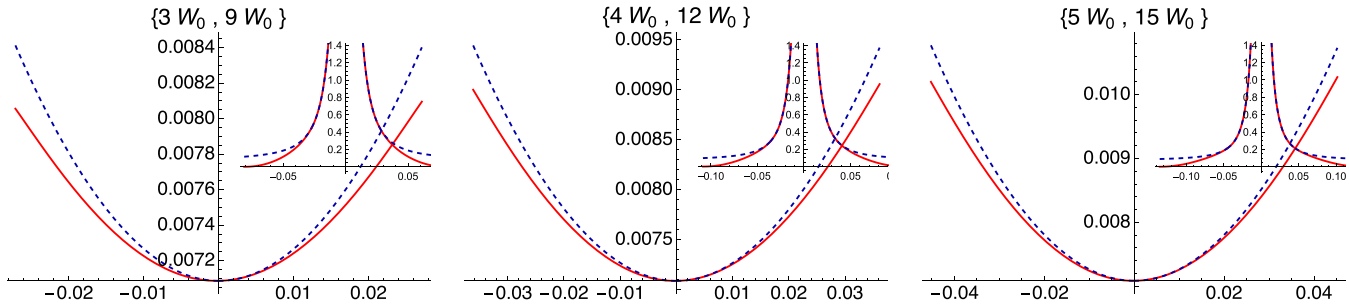

FIG. 6. These figures are for the asymmetric Fermi-liquid model Eq. (11) with parameters given in Eq. (15). The reconstructed self-energy $\rho_\Sigma(\vec{k}_F,\omega)+\frac{\eta}{\pi}$ (red curves) using the soft cutoff Eq. (9) compared with the exact value in the dashed blue curves. The two parameters relating to the soft cutoff Eq. (9) are indicated in curly brackets. The three insets show the exact spectral function in dashed blue and the cutoff included spectral function A' of Eq. (7) in the red curves. Here upper cutoff is 3 times the lower one, and shows a fair improvement over the results of Fig. 5 where the upper cutoff is only twice the lower one. Here W_0 is ∼9 meV.

and the reconstructed self-energy with a few typical window parameters also in Fig. 7. The reconstructed self-energy is displayed in Fig. 8.

The functional form of ρ_Σ in the M-FL-a model Eq. (12) has a flat portion in its minima, which is reflected in the lowest-energy behavior as seen in Fig. 8. The M-FL-b model Eq. (13) on the other hand avoids this flat feature. For the M-FL-b model, the parameters used are

$$\epsilon_0 = 1.8, \quad \eta = 0.02, \quad \tau = 0.015; \alpha_z = 1 \tag{17}$$

leading to a width $W_0 = 11$ meV. We now show the spectral function and the real part of G in Fig. 9 and the reconstructed self-energy in Fig. 10 for the M-FL-b model given by Eq. (13), with a few typical window parameters.

C. A non-Fermi-liquid model

For the N-FL model Eq. (14), the parameters used are

$$\epsilon_0 = 1.8, \eta = 0.02, \tau = 0.02; \alpha_z = 1 \tag{18}$$

leading to a width $W_0 = 10$ meV. We next display the spectral function and the real part of G in Fig. 11 and the reconstructed self-energy Fig. 12 for the N-FL model given by Eq. (14), with a few typical window parameters. We now show the reconstructed self-energy with a few typical window parameters

III. COMMENTS AND CONCLUSIONS

The proposal for reconstructing the self-energy from the spectral function made in this work in Sec. I B, was illustrated above in Sec. II in a set of figures (Figs. 3–12) using three typical models with different predictions. These figures show that an experimental implementation of the proposal could lead to interesting insights about the nature of quantum matter.

Different theoretical approaches to the strong correlation problem, originally inspired by the high-T_c cuprates but branching out to a much broader portfolio of materials in recent years, lead to a variety of different self-energies; some of them are discussed in this work. Fundamental questions about the nature of these quantum materials remain open in most cases; it is unclear whether they constitute some variety of Fermi liquids, or some variety of non-Fermi liquids. While the resistivity is often used to discriminate between these states of matter, it is a much more complex probe to interpret robustly. On the other hand a much more direct avenue to answer the above basic question is to study the (imaginary part of the) self-energy at low energies. At present it seems that no decisive tests using experimental ARPES data has been carried out in that direction. This is the motivation for the present paper, where we present a method to extract the low-ω self-energy from ARPES-derived spectral function. It is based

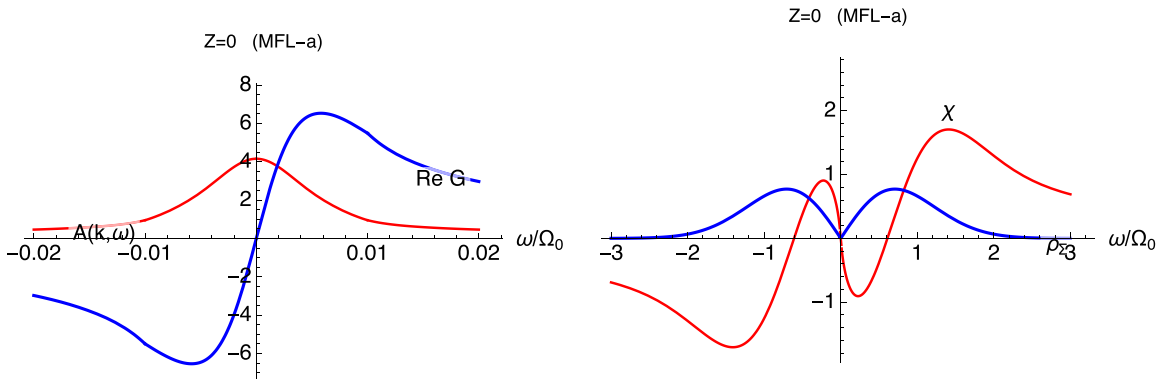

FIG. 7. These figures are for the marginal Fermi-liquid-a model Eq. (12) with parameters given in Eq. (16). (Left) The spectral function $A(\vec{k}_F,\omega)$ and the $Re\,G(\vec{k}_F,\omega)$ and (right) the imaginary self-energy $\rho_\Sigma(\vec{k}_f,\omega)$ and $\chi(\vec{k}_F,\omega)$ for the M-FL-a model Eq. (12), calculated from Eqs. (41), (38), (48). Here the spectral peak width W_0 is ∼12 meV.

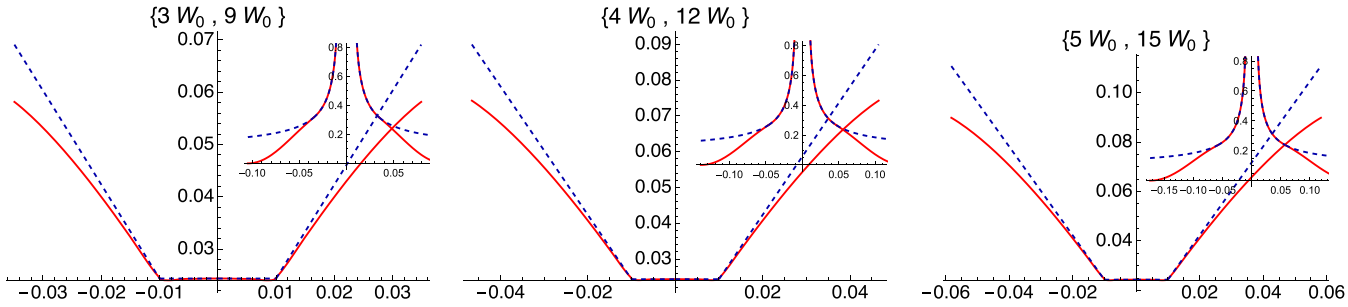

FIG. 8. These figures are for the marginal Fermi-liquid-a model Eq. (12) with parameters given in Eq. (16). The reconstructed self-energy $\rho_\Sigma(\vec{k}_F,\omega)+\frac{\eta}{\pi}$ (red curves) using the soft cutoff Eq. (9) compared with the exact value in the dashed blue curves. The two parameters relating to the soft cutoff Eq. (9) are indicated in curly brackets. The three insets show the exact spectral function in dashed blue and the cutoff included spectral function A' of Eq. (7) in the red curves. Here upper cutoff is 3 times the lower one. Here W_0 is ∼12 meV.

on the helpful Theorem 1, which assures us that the inversion method used has least error at low energies.

The proposal presented in Sec. I B is to use Eq. (3) and a suitable windowing of the spectral function, analogous to that in Eq. (9) to infer the imaginary self-energy from the ARPES-derived spectral function. We provide several examples in Sec. II that show that the different model systems yield distinguishably different low-energy self-energies.

We conclude with a few comments:

(1) The suggested inversion process can be used to estimate the elastic scattering parameter η, from the T-independent part of the derived self-energy as $\omega\to 0$. For this purpose one can use the inversion data at a few (typically two or three) distinct temperatures together with Eqs. (36), (37) to deduce η.

(2) The observed peaks in the spectral function at $\vec{k}_F$ are expected to have a T-dependent shift given in Eqs. (26), (49), (51). The shift in Eq. (B18) contains the chemical potential part that can be estimated from the thermopower. The remainder has two terms in it, but is expected to be dominated by the term containing the asymmetry parameter α [see Eq. (11)]. This can be a useful way to estimate α from the low-energy experiments.

(3) The role of noise in the spectral function warrants mention; the Theorem 1 also applies to the noise. This offers hope that at low energies, the errors due to noise are least.

(4) While we have focused on $\vec{k}=\vec{k}_F$ here, it might be possible to explore departures from the Fermi surface if high-quality spectral functions are obtainable from the intensities over a wide range of energies. We are suggesting that $\vec{k}$, chosen in the proximity of $\vec{k}_F$, should suffice for estimating the crucial frequency dependence $\rho_\Sigma(\vec{k},\omega)$ near $\vec{k}_F$.

(5) The method described here requires the self-energy to be diagonal in spin-space. It does not extend to arbitrary $\vec{k}$ in a superconducting state, where the self-energy is a 2×2 matrix on account of the anomalous (i.e. pairing) part. However an important exception is the nodal direction in 2-d d-wave superconductor, where the off-diagonal matrix elements of the self-energy vanish, and hence our inversion method is applicable.

APPENDIX A: SUMMARY OF BASIC DEFINITIONS

In this section we reorganize the familiar properties of the Green's function [11–13] to define specific quantities used in our analysis. We start with the standard expression for the retarded Green's function $G^{-1}(\vec{k},\omega_c)=\omega_c+\mu-\varepsilon_k-\Sigma(\vec{k},\omega_c)$, with $\omega_c=\omega+i0^+$ [11–13]. Emphasizing the role of the spectral density of the self-energy $\rho_\Sigma(\vec{k},\omega)=-\frac{1}{\pi}\mathrm{Im}\,\Sigma(\vec{k},\omega_c)$, we decompose

$$\Sigma(k,\omega_c)=(1-\alpha_z)(\omega+\mu)+\Sigma_*(\vec{k})-i\pi\rho_\Sigma(\vec{k},\omega)+\chi(\vec{k},\omega), \tag{A1}$$

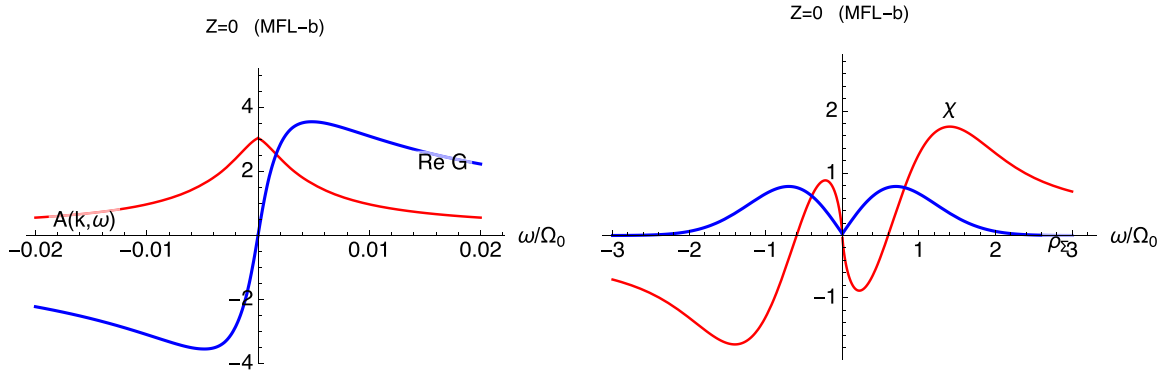

FIG. 9. These figures are for the marginal Fermi-liquid-b model Eq. (13) with parameters given in Eq. (17). (Left) The spectral function $A(\vec{k}_F,\omega)$ and the $Re\,G(\vec{k}_F,\omega)$ and (right) the imaginary self-energy $\rho_\Sigma(\vec{k}_f,\omega)$ and $\chi(\vec{k}_F,\omega)$, calculated from Eqs. (41), (38), (48), using parameters given in Eq. (17). Here the spectral peak width W_0 is ∼11meV.

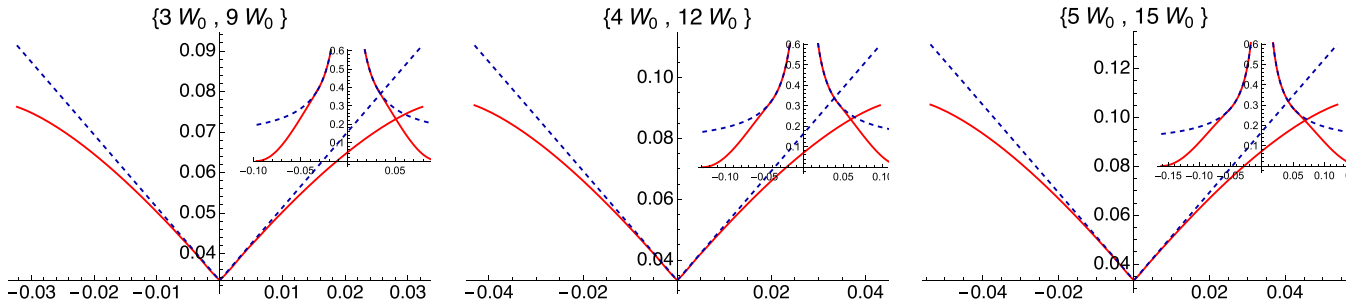

FIG. 10. These figures are for the marginal Fermi-liquid-b model Eq. (13) with parameters given in Eq. (17). The reconstructed self-energy $\rho_\Sigma(\vec{k}_F,\omega)+\frac{\eta}{\pi}$ (red curves) using the soft cutoff Eq. (9) compared with the exact value in the dashed blue curves. The two parameters relating to the soft cutoff Eq. (9) are indicated in curly brackets. The three insets show the exact spectral function in dashed blue and the cutoff included spectral function A' of Eq. (7) in the red curves. Here upper cutoff is 3 times the lower one. Here W_0 is ∼11 meV. Note the difference in the shape at low ω from that in Fig. 8 This version has a linear behavior down to the lowest energy.

where χ can be obtained from the Hilbert transform of $\rho_\Sigma(\vec{k},\omega)$ as

$$\chi(\vec{k},\omega)=\int d\nu\frac{\rho_\Sigma(\vec{k},\nu)}{\omega-\nu}. \tag{A2}$$

By definition $\lim_{\omega\to\infty}\chi(\vec{k},\omega)\to 0$ (assuming an integrable ρ_Σ). Here Σ_* is the static part of the self-energy, analogous to the Hartree-Fock term, which remains finite as $\omega\to\infty$. It cannot be deduced from $\rho_\Sigma(\vec{k},\omega)$, we see below that it can be absorbed in the measurable shifts of the peaks as defined below in Eqs. (26), (27). The constant α_Z is given by

$$\alpha_z=1,\ \text{canonical (Hubbard-type) fermions} \tag{A3}$$

$$\alpha_z=\frac{1}{1-\frac{1}{2}n},\ \text{Gutzwiller projected } t\text{-}J\text{-type fermions} \tag{A4}$$

and reflects the basic nature of the fermions in various models [14]. Using this decomposition we write

$$G^{-1}(\vec{k},\omega_c)=\alpha_z(\omega_c+\mu)-\varepsilon_{\vec{k}}-\Sigma_*(\vec{k})-\chi(\vec{k},\omega)+i\pi\rho_\Sigma(\vec{k},\omega). \tag{A5}$$

We rewrite this expression using the basic idea that at $T=0$ on the Fermi surface $G(\vec{k}_F,\omega)$ has a pole at $\omega=0$. Since $\rho_\Sigma(\vec{k}_F,0)$ vanishes,

$$\alpha_z\times\mu|_{T=0}=\varepsilon_{\vec{k}_F}+(\Sigma_*(\vec{k}_F)+\chi(\vec{k}_F,0))|_{T=0}, \tag{A6}$$

which can be used in Eq. (A5) to rewrite it as

$$G^{-1}(\vec{k},\omega_c)=\omega_c\alpha_z+\Delta\omega-\Delta k+\chi(\vec{k},0)-\chi(\vec{k},\omega)+i\pi\rho_\Sigma(\vec{k},\omega), \tag{A7}$$

where the real functions $\Delta\omega$ the energy shift, and Δk the momentum shift are give by

$$\Delta\omega=\alpha_z(\mu-\mu|_{T=0})+[\Sigma_*(\vec{k}_F)|_{T=0}-\Sigma_*(\vec{k}_F)]+[\chi(\vec{k}_F,0)|_{T=0}-\chi(k_F,0)] \tag{A8}$$

$$\Delta k=(\varepsilon_{\vec{k}}-\varepsilon_{\vec{k}_F})+[\Sigma_*(\vec{k})-\Sigma_*(\vec{k}_F)]+[\chi(\vec{k},0)-\chi(\vec{k}_F,0)]. \tag{A9}$$

By their definitions, $\Delta\omega$ vanishes at $T=0$, while Δk vanishes at $\vec{k}_F$. At low T $\Delta\omega$ is expected to be small and may be estimated from the thermopower S using the approximate Kelvin relation for thermopower $S_{\text{Kelvin}}=\frac{-1}{q_e}(\frac{\partial\mu(T)}{\partial T})|_{N,V}$, where q_e is the electron charge.

The momentum shift Δk (at arbitrary T) is of $\mathcal{O}(|\vec{k}-\vec{k}_F|)$ for $\vec{k}$ near $\vec{k}_F$. We now split $G(\omega+i0^+)$ into its real and

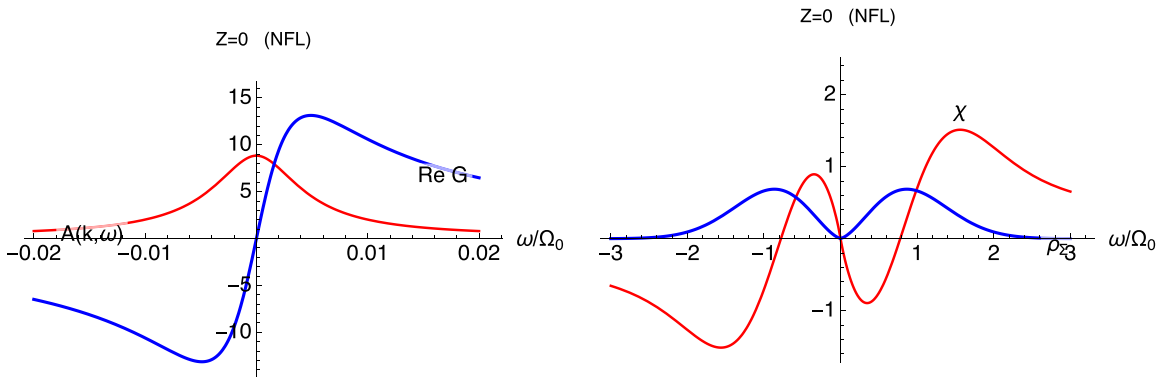

FIG. 11. These figures are for the non-Fermi-liquid model Eq. (14) with parameters given in Eq. (18). (Left) The spectral function $A(\vec{k}_F,\omega)$ and the *Re* $G(\vec{k}_F,\omega)$ and (right) the imaginary self energy $\rho_\Sigma(\vec{k}_f,\omega)$ and $\chi(\vec{k}_F,\omega)$, calculated from Eqs. (41), (38), (48), using parameters given in Eq. (18). Here the spectral peak width W_0 is ∼10 meV.

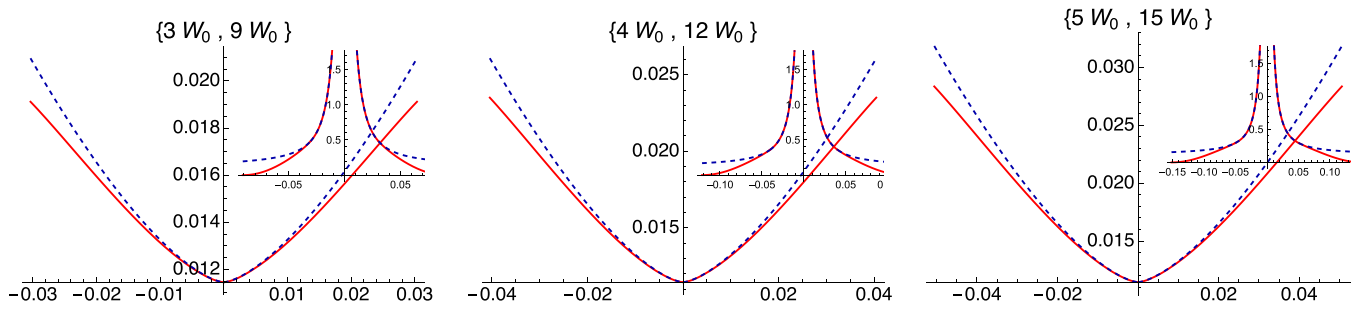

FIG. 12. These figures are for the non-Fermi-liquid model Eq. (14) with parameters given in Eq. (18). The reconstructed self-energy $\rho_\Sigma(\vec{k}_F,\omega)+\frac{\eta}{\pi}$ (red curves) using the soft cutoff Eq. (9) compared with the exact value in the dashed blue curves. The two parameters relating to the soft cutoff Eq. (9) are indicated in curly brackets. The three insets show the exact spectral function in dashed blue and the cutoff included spectral function A' of Eq. (7) in the red curves. Here upper cutoff is 3 times the lower one. Here W_0 is ∼10 meV.

imaginary parts as

$$G(\vec{k},\omega_c)=\mathrm{Re}\,G(\vec{k},\omega)-i\pi A(\vec{k},\omega) \tag{A10}$$

so that the spectral function $A(\vec{k},\omega)=-\frac{1}{\pi}\mathrm{Im}\,G(\vec{k},\omega)$. Using Eq. (A7) we get

$$A(\vec{k},\omega)=\frac{\rho_\Sigma(\vec{k},\omega)}{\{\alpha_z\omega+\Delta\omega-\Delta k+\chi[\vec{k},0)-\chi(\vec{k},\omega)]\}^2+\pi^2\rho_\Sigma^2(\vec{k},\omega)}, \tag{A11}$$

and

$$\mathrm{Re}\,G(\vec{k},\omega)=\frac{\{\alpha_z\omega+\Delta\omega-\Delta k+\chi[(\vec{k},0)-\chi(\vec{k},\omega)]\}}{\{\alpha_z\omega+\Delta\omega-\Delta k+\chi[(\vec{k},0)-\chi(\vec{k},\omega)]\}^2+\pi^2\rho_\Sigma^2(\vec{k},\omega)}. \tag{A12}$$

We now recall that the real and imaginary parts of the (causal) retarded Green's function $G(\omega+i0^+)$ are also related by the Kramers-Kronig relation

$$\mathrm{Re}\,G(\vec{k},\omega)=\int d\nu\frac{A(\vec{k},\nu)}{\omega-\nu}, \tag{A13}$$

so that a complete knowledge of A suffices to determine Re G.

Now moving in a slightly different direction, taking the imaginary part of Eq. (A5) we get

$$\rho_\Sigma(\vec{k},\omega)=\frac{1}{\pi}\mathrm{Im}\,G^{-1}(\vec{k},\omega). \tag{A14}$$

Using Eq. (A10) this give ρ_Σ in terms of $A(\vec{k},\omega)$ and Re$G(\vec{k},\omega)$ as

$$\rho_\Sigma(\vec{k},\omega)=\frac{A(\vec{k},\omega)}{\{\mathrm{Re}\,G(\vec{k},\omega)\}^2+\{\pi A(\vec{k},\omega)\}^2}. \tag{A15}$$

This equation asserts that if we know the spectral function $A(\vec{k},\omega)$ for all ω, we can retrieve $\rho_\Sigma(\vec{k},\omega)$, since the Re G can be inferred through the Hilbert transform Eq. (A13). Relabeling Re G as $\Phi_{\vec{k}}(\omega)$ gives Eq. (3).

APPENDIX B: DETAILS OF THE ASYMMETRIC FERMI-LIQUID MODEL

1. Scaled variables and expressions for Hilbert transforms

Let us consider a FL-type model with a cubic asymmetry: We denote

$$\bar{\omega}=\frac{\omega}{\Omega_0},\quad \bar{\tau}=\frac{\pi k_BT}{\Omega_0},\quad \bar{A}=\frac{A}{\Omega_0},\quad \bar{\epsilon}_0=\frac{\epsilon_0}{\Omega_0} \tag{B1}$$

$$\rho_\Sigma(\vec{k}_F,\omega,T)=\epsilon_0(\bar{\tau}^2+\bar{\omega}^2)(1-\alpha\bar{\omega})e^{-\bar{\omega}^2}. \tag{B2}$$

We scale the self-energy with Ω_0 so that

$$\bar{\rho}_\Sigma(\vec{k}_F,\bar{\omega},\bar{\tau})=\bar{\epsilon}_0\big(\bar{\tau}^2+\bar{\omega}^2\big)(1-\alpha\bar{\omega})e^{-\bar{\omega}^2}. \tag{B3}$$

In this and also in other models we implicitly add an elastic scattering term η/π to $\rho_\Sigma(\vec{k},\omega)$,

$$\rho_\Sigma(\vec{k},\omega)|_{\mathrm{Total}}=\rho_\Sigma(\vec{k},\omega)+\frac{\eta}{\pi}, \tag{B4}$$

as shown in Eq. (B15). This term arises from impurity scattering [15], and is found to be useful in distinguishing between ARPES at different incident photon energies [10]. Its corresponding real part arising from causality, is dropped since the bandwidth for this term is very large, typically a few eV's. In practical terms adding η is equivalent to increasing the physical temperature T to $\sqrt{T^2+\frac{\eta}{\pi^3\epsilon_0}}$, usually this is a small effect.

In summary the model has the following parameters:

(1) strength of self energy: ϵ_0;

(2) reduced temperature: $\bar{\tau}$;

(3) cubic asymmetry: α;
(4) large energy scale: Ω_0;
(5) elastic scattering scale: $\bar{\eta}$.

We rewrite Eq. (B3) as

$$\bar{\rho}_\Sigma(\vec{k}_F, \bar{\omega}, \bar{\tau}) = \bar{\epsilon}_0(\bar{\tau}^2\rho_0(\bar{\omega}) + \rho_2(\bar{\omega}) - \alpha[\bar{\tau}^2\rho_1(\bar{\omega}) + \rho_3(\bar{\omega})]), \tag{B5}$$

where

$$\rho_m(\bar{\omega}) = e^{-\bar{\omega}^2} \times \bar{\omega}^m. \tag{B6}$$

We write its Hilbert transform as

$$\begin{aligned}\chi(\vec{k}_F, \omega, T) &= \int_{-\infty}^{\infty} \frac{\rho_\Sigma(\vec{k}_F, x, T)}{\omega - x} dx \\ &= \Omega_0 \int_{-\infty}^{\infty} \frac{\bar{\rho}_\Sigma(\vec{k}_F, \bar{x}, \bar{\tau})}{\bar{\omega} - \bar{x}} d\bar{x}.\end{aligned} \tag{B7}$$

By plugging in for ρ_Σ we get

$$\begin{aligned}\bar{\chi}(\vec{k}_F, \bar{\omega}, \bar{\tau}) &\equiv \frac{1}{\Omega_0}\chi(\vec{k}_F, \omega, T) \\ &= \bar{\epsilon}_0(\bar{\tau}^2\chi_0(\bar{\omega}) + \chi_2(\bar{\omega}) - \alpha[\bar{\tau}^2\chi_1(\bar{\omega}) + \chi_3(\bar{\omega})]),\end{aligned} \tag{B8}$$

where

$$\chi_m(\bar{\omega}) = \int_{-\infty}^{\infty} \frac{\rho_m(\bar{x})}{\bar{\omega} - \bar{x}} d\bar{x}. \tag{B9}$$

The evaluation of χ_m for even m follows from the identity

$$\int_{-\infty}^{\infty} \frac{e^{-\alpha y^2}}{x - y} dy = 2\sqrt{\pi} D_F(\sqrt{\alpha} x) \quad \text{with } \alpha > 0, \tag{B10}$$

by differentiating under the integral sign with respect to α, and where D_F is the Dawson function

$$D_F(x) = e^{-x^2} \int_0^x e^{t^2}\, dt. \tag{B11}$$

For odd m we use the method of partial fractions to depress the order m by one, and then use the above scheme for order $m - 1$. In this way we find

$$\begin{aligned}\chi_0(x) &= \sqrt{\pi} 2 D_F(x) \\ \chi_1(x) &= \sqrt{\pi}[2x D_F(x) - 1] \\ \chi_2(x) &= \sqrt{\pi} x[2x D_F(x) - 1] \\ \chi_3(x) &= \sqrt{\pi}\big[2x^3 D_F(x) - x^2 - \tfrac{1}{2}\big].\end{aligned} \tag{B12}$$

The Dawson function has a series expansion for small x

$$D_F(x) \sim x - \tfrac{2}{3}x^3 + O(x^5). \tag{B13}$$

We read off Z from this as

$$\begin{aligned}\frac{1}{Z} &= \alpha_z - \partial_\omega \chi(\vec{k}_F, \omega, T) \\ &= \alpha_z - \bar{\epsilon}_0(\bar{\tau}^2\chi_0'(\bar{\omega}) + \chi_2'(\bar{\omega}) - \alpha[\bar{\tau}^2\chi_1'(\bar{\omega}) + \chi_3'(\bar{\omega})])|_{\bar{\omega}\to 0} \\ &= \alpha_z + \sqrt{\pi}\bar{\epsilon}_0(1 - 2\bar{\tau}^2),\end{aligned} \tag{B14}$$

where the prime denotes a derivative in the second line. In dimensionless (i.e., scaled) units with $\bar{\rho}_\Sigma = \Omega_0\rho_\Sigma$ we write

$$\bar{A}(\vec{k}_F, \bar{\omega}, \bar{\tau}) = \frac{\frac{\bar{\eta}}{\pi} + \bar{\rho}_\Sigma(\vec{k}_F, \bar{\omega}, \bar{\tau})}{\big[\frac{\bar{\omega}}{Z(\bar{\omega})} - \Delta\bar{\omega}(\bar{\tau})\big]^2 + [\bar{\eta} + \pi\bar{\rho}_\Sigma(\vec{k}_F, \bar{\omega}, \bar{\tau})]^2}, \tag{B15}$$

where we have added an elastic scattering constant $\bar{\eta}$ to the $\mathrm{Im}\Sigma$, and thereby a constant $\frac{\bar{\eta}}{\pi}$ to $\bar{\rho}_\Sigma$ here. It is important to note that the total self-energy Eq. (B4) deduced by inverting the A of Eq. (B15), will contain an added contribution of $\frac{\eta}{\pi}$ to ρ_Σ. This is commented on in Sec. III, and made specific in the captions of figures Figs. 4, 5, 6, 8, 10, 12 in the paper.

Also note that

$$\begin{aligned}\Delta\bar{\omega}(\bar{\tau}) = &\frac{1}{\Omega_0}(\mu(0) - \mu(T)) + \frac{1}{\Omega_0}(\Sigma_*(\vec{k}_F, T) - \Sigma_*(\vec{k}_F, 0)) \\ &+ (\bar{\chi}(\vec{k}_F, 0, \bar{\tau}) - \bar{\chi}(\vec{k}_F, 0, 0)).\end{aligned} \tag{B16}$$

We note the lowest-order $\bar{\omega}$ expansions

$$\begin{aligned}\bar{\rho}_\Sigma(\vec{k}_F, \omega) &\sim \bar{\epsilon}_0(\bar{\omega}^2 + \bar{\tau}^2)(1 - \alpha\bar{\omega}) \\ \bar{\chi}(\bar{\omega}, \bar{\tau}) &\sim \tfrac{1}{2}\alpha\sqrt{\pi}\bar{\epsilon}_0(1 + 2\bar{\tau}^2) \\ &\quad - \sqrt{\pi}\bar{\epsilon}_0(1 - 2\bar{\tau}^2)\bar{\omega} + \mathcal{O}(\bar{\omega}^2).\end{aligned} \tag{B17}$$

It follows that

$$\begin{aligned}\Delta\bar{\omega}(\bar{\tau}) = &\frac{1}{\Omega_0}[\mu(0) - \mu(T)] + \frac{1}{\Omega_0}[\Sigma_*(\vec{k}_F, T) - \Sigma_*(\vec{k}_F, 0)] \\ &+ \alpha(\sqrt{\pi}\bar{\epsilon}_0\bar{\tau}^2).\end{aligned} \tag{B18}$$

Therefore the asymmetry parameter α shows up in $\Delta\bar{\omega}$ linearly. In some situations it might be reasonable to assume that this term dominates over the others, and if this is prevails then one can expect to extract α from the shift of the spectral peak at $\vec{k}_F$ as a function of T.

2. Useful properties of the peaks very close to $\omega = 0$

Here we simplify the above expressions in the neighborhood of $\omega = 0$. With

$$Z = \frac{1}{\alpha_z + \sqrt{\pi}\bar{\epsilon}_0(1 - 2\bar{\tau}^2)} \tag{B19}$$

$$\Gamma_0 = Z\bar{\eta} + Z\bar{\epsilon}_0\pi\bar{\tau}^2 \tag{B20}$$

$$\Gamma_2 = Z\bar{\epsilon}_0\pi \tag{B21}$$

we get

$$\bar{A}(\vec{k}_F, \bar{\omega}) \sim \frac{Z}{\pi}\frac{\Gamma_0 + \Gamma_2\bar{\omega}^2}{(\Gamma_0 + \Gamma_2\bar{\omega}^2)^2 + (\bar{\omega} - Z\Delta\bar{\omega})^2}. \tag{B22}$$

Further simplifying to a small shift $Z\Delta\bar{\omega} \ll 1$

$$\bar{A}(\vec{k}_F, \bar{\omega}) \sim \frac{Z}{\pi}\frac{\Gamma_0 + \Gamma_2\bar{\omega}^2}{(\Gamma_0 + \Gamma_2\bar{\omega}^2)^2 + \bar{\omega}^2} \tag{B23}$$

so that $\{\bar{A}\}_{\max} = \bar{A}(\vec{k}_F, 0) = \frac{Z}{\pi\Gamma_0}$. We note that the scaled width (FWHM) of the spectral peak used in the analysis is given by

$$\bar{W}_0 = 2\sqrt{-\frac{1}{2\Gamma_2^2} + \frac{1}{2\Gamma_2^2}\big(1 + 4\Gamma_0^2\Gamma_2^2\big)^{\frac{1}{2}}}. \tag{B24}$$

[1] X. Zhou, S. He, G. Liu, L. Zhao, Li Yu, and W. Zhang, New developments in laser-based photoemission spectroscopy and its scientific applications: A key issues review, Rep. Prog. Phys. **81**, 062101 (2018); J. A. Sobota, Y. He, and Z. X. Shen, Angle-resolved photoemission studies of quantum materials, Rev. Mod. Phys. **93**, 025006 (2021).

[2] T. Valla, A. V. Fedorov, P. D. Johnson, B. O. Wells, S. L. Hubert, Q. Li, G. D. Gu, and N. Koshizuka, Evidence for quantum critical behavior in the optimally doped cuprate $Bi_2Sr_2CaCu_2O_{8+\delta}$, Science **285**, 2110 (1999).

[3] J. Jang, H. M. Yoo, L. Pfeiffer, K. West, K. W. Baldwin, and R. Ashoori, Full momentum and energy resolved spectral function of a 2D electronic system, Science **358**, 901 (2017).

[4] This relation was noted and used in B. S. Shastry, Anatomy of the self energy, Phys. Rev. B **84**, 165112 (2011) [see Eqs. (22), (23)], and in subsequent work of our group [7]. Earlier work employing this relation could not be traced by the author.

[5] The removal of the Fermi function and an instrumental resolution from the ARPES intensity is a precondition for obtaining the electron spectral function. This important problem has been extensively discussed in literature, see, e.g., Refs. [1,6]. We should note that in the present work, the focus on the spectra at $\vec{k} = \vec{k}_F$ at very low ω implies that the symmetrization of $A(\vec{k}_F, \omega)$, as suggested in Norman *et al.*, Destruction of the Fermi surface in underdoped high-Tc superconductors, Nature (London) **392**, 157 (1998). This process is sometimes regarded [6,7] as being unduly biased by expectations of particle hole symmetry, may be harmless due to the smallness of the effects of asymmetry in this energy regime.

[6] J. D. Rameau, H. B. Yang, and P. D. Johnson, Application of the Lucy–Richardson deconvolution procedure to high resolution photoemission spectra, J. Electron Spectrosc. Relat. Phenom. **181**, 35 (2010).

[7] B. S. Shastry, Extremely correlated fermi liquids, Phys. Rev. Lett. **107**, 056403 (2011); P. Mai and B. S. Shastry, Extremely correlated fermi liquid of t-J model in two dimensions, Phys. Rev. B **98**, 205106 (2018); B. S. Shastry, Dynamical particle hole asymmetry in cuprate superconductors, Phys. Rev. Lett. **109**, 067004 (2012); B. S. Shastry and P. Mai, Aspects of the normal state resistivity of cuprate superconductors, Phys. Rev. B **101**, 115121 (2020).

[8] C. M. Varma, P. B. Littlewood, S. Schmitt-Rink, E. Abrahams, and A. E. Ruckenstein, Phenomenology of the normal state of Cu-O high-temperature superconductors, Phys. Rev. Lett. **63**, 1996 (1989).

[9] D. Chowdhury, A. Georges, O. Parcollet, and S. Sachdev, Sachdev-Ye-Kitaev models and beyond: Window into non-Fermi liquids, Rev. Mod. Phys. **94**, 035004 (2022); S. Sachdev and J. Ye, Gapless spin-fluid ground state in a random quantum Heisenberg magnet, Phys. Rev. Lett. **70**, 3339 (1993).

[10] J. D. Koralek, J. F. Douglas, N. C. Plumb, Z. Sun, A. V. Federov, M. M. Murnane, H. C. Kapteyn, S. T. Cundiff, Y. Aiura, K. Oka, H. Eisaki, and D. S. Dessau, Laser based angle-resolved photoemission, the sudden approximation, and quasiparticle-like spectral peaks in $Bi_2Sr_2CaCu_2O_8$, Phys. Rev. Lett. **96**, 017005 (2006); G. H. Gweon, B. S. Shastry, and G. D. Gu, Extremely correlated fermi liquid description of normal state ARPES in cuprates, **107**, 056404 (2011).

[11] A. A. Abrikosov, L. Gorkov, and I. Dzyaloshinski, *Methods of Quantum Field Theory in Statistical Physics* (Prentice-Hall, Englewood Cliffs, 1963).

[12] A. L. Fetter and J. D. Walecka, *Quantum Theory of Many-Particle Systems* (McGraw-Hill, New York, 1971).

[13] P. Nozières, in *Theory of Interacting Fermi Systems* (W. A. Benjamin, New York, 1964).

[14] The constant α_z equals unity in canonical models, but takes on a different value for Gutzwiller projected electrons. The main reason is that in the latter models, the Green's function used refers to only the lower Hubbard band states. A weight of $\frac{n}{2}$ belonging to doubly occupied states, i.e., the upper Hubbard band are thrown out. This is discussed further in B. S. Shastry and E. Perepelitsky, Low energy physics of the t-J model in $d = \infty$ using extremely correlated fermi liquid theory: cutoff second order equations, Phys. Rev. B **94**, 045138 (2016).

[15] E. Abrahams and C. M. Varma, What angle-resolved photoemission experiments tell about the microscopic theory for high-temperature superconductors, Proc. Natl. Acad. Sci. USA **97**, 5714 (2000).